Calculation of Elastic and Inelastic Proton Scattering with a Generalized Optical Model

B. Buck
Oak Ridge National Laboratory, Oak Ridge, Tennessee*
(Received 28 November 1962)

An extension of the optical model is considered in which a state of quadrupole collective motion is strongly coupled to the nuclear ground state. The calculations include a spin-orbit potential and the simultaneous coupled differential equations of the problem are solved numerically on a high-speed computer. Experimental data on the scattering of medium energy protons from Ti, Cr, Fe, Ni, and Zn are analyzed. A good average optical potential is determined and conclusions are drawn about the energy dependence of the parameters. Evidence is presented for the validity of the collective model. Nuclear deformabilities derived by fitting the inelastic differential cross sections are in good agreement with those determined by electromagnetic methods. Various limitations and ambiguities of the model are discussed and possible improvements are indicated.

1. INTRODUCTION

THE optical model for the elastic scattering of nucleons by complex nuclei has been very successful in the last few years. As more and better data became available, it has proved possible to find good average parameters which enable one to calculate accurately the expected elastic scattering for a wide range of nuclei. More important, it has become feasible to study the deviations of the results for individual nuclei away from the average parameters and to correlate these with nuclear structure effects.[1] This treatment of the elastic scattering appears to be applicable to any nucleus, although usually it does not work too well for light nuclei ($A<30$). It is the purpose of this paper to consider a generalization of the optical model which will make possible the simultaneous calculation of the elastic scattering of nucleons and the inelastic scattering to low-lying excited states of the target nucleus.

All even-even nuclei have ground state spin 0^+, and a large proportion of these have low excited states of spins 0^+, 2^+, 3^-, 4^+, etc., which can be interpreted as nuclear collective motions. The majority of even-even nuclei have a quadrupole state as the first excited level and this level is often strongly populated by medium energy neutron or proton bombardment. Hence, the most obvious generalization of the optical model is a calculation in which a nuclear ground state of spin 0^+ and a collective state of spin 2^+ are included explicitly. Since the excitation of first 2^+ states by nucleons varies strongly and erratically from nucleus to nucleus, one may hope by this means to remove one source of fluctuation in the optical-model parameters. One should also be able to correlate the nucleon inelastic scattering with the results of Coulomb excitation measurements and $B(E2)$ determinations.

* Operated by Union Carbide Nuclear Company for the U. S. Atomic Energy Commission.

[1] F. Perey (private communication) and (to be published).

2. DESCRIPTION OF CALCULATION

The methods described here are, in principle, very similar to those of Chase *et al.*,[2] but the formalism is extended to include the consideration of charged incident particles, spin-orbit effects, and easy specialization to rotational, vibrational, or single-particle excitation models.

In order to set up the generalized optical-model calculation, we start with the Schrödinger equation for the system consisting of an incident nucleon and a target nucleus. We work in the center-of-mass coordinate frame so that only reduced masses and relative energies and momenta appear in the equations. The wave equation is

$$[H_N(\xi)+T+V(\mathbf{r},\xi)]\Psi(\mathbf{r},\xi)=E\Psi(\mathbf{r},\xi). \quad (1)$$

Here, $\mathbf{r}$ denotes the coordinates of the incident particle, ξ stands for the internal coordinates of the target nucleus, $H_N(\xi)$ is the target nuclear Hamiltonian, T is the kinetic energy operator for the relative motion, $V(\mathbf{r},\xi)$ is the interaction energy between particle and nucleus, $\Psi(\mathbf{r},\xi)$ is the complete wave function of the system, and E is the total energy. $\Psi(\mathbf{r},\xi)$ is expanded in eigenstates of the total angular momentum,

$$\Psi(\mathbf{r},\xi)=\sum_{JM} a_{JM}\psi_J{}^M(\mathbf{r},\xi). \quad (2)$$

We assume that $\psi_J{}^M(\mathbf{r},\xi)$, for each entrance channel (Ijl), can be adequately described by the superposition of the elastic and inelastic scattering states, as follows:

$$\psi_J{}^M(\mathbf{r},\xi)=\frac{1}{r}[f_{Ijl}{}^J(r)\phi_{Ijl}{}^{JM}(\hat{r},\xi)+\sum_{j'l'} f_{I'j'l'}{}^J(r)\phi_{I'j'l'}{}^{JM}(\hat{r},\xi)], \quad (3)$$

where

$$\phi_{Ijl}{}^{JM}(\hat{r},\xi)=\sum_{k\lambda\mu} C_{Mkm}{}^{JIj}C_{m\lambda\mu}{}^{jls}\times\Psi_I{}^k(\xi)\{i^l Y_l{}^\lambda(\hat{r})\}\chi_s{}^\mu. \quad (4)$$

[2] D. M. Chase, L. Wilets, and A. R. Edmonds, Phys. Rev. **110**, 1080 (1958).

The functions, $f_{Ijl}{}^J(r)$, are the radial wave functions of particles scattered from nuclear states with spin I, partial wave l, relative angular momentum $j=l\pm\frac{1}{2}$, and total angular momentum J. The functions $\phi_{Ijl}{}^{JM}(\hat{r},\xi)$ represent the nuclear wave functions, $\Psi_I{}^k(\xi)$, vector coupled to the spin-angular parts of the incident particle wave functions, $\{i^l Y_l{}^\lambda(\hat{r})\}\chi_s{}^\mu(s=\frac{1}{2})$. Other reaction channels, and hence the rest of the total wave function, are taken into account only in a general way via the later introduction of complex optical potentials.

Insertion of the angular momentum eigenfunctions in the wave equation yields, after a little manipulation, the following set of coupled differential equations for the radial functions $f_{Ijl}{}^J(r)$ and $f_{I'j'l'}{}^J(r)$, valid for $I=0$, $I'\neq 0$

$$[T_l+V_{Ijl:Ijl}{}^J(r)-E]f_{Ijl}{}^J(r)+\sum_{j'l'}V_{Ijl:I'j'l'}{}^J f_{I'J'l'}{}^J(r)=0, \quad (5)$$

$$[T_{l'}+V_{I'j'l':I'j'l'}{}^J(r)-E']f_{I'j'l'}{}^J(r)+\sum_{j''l''}V_{I'j'l':I'j''l''}{}^J(r)f_{I'j''l''}{}^J(r)+V_{I'j'l':Ijl}{}^J(r)f_{Ijl}{}^J(r)=0, \quad (6)$$

where

$$T_l=\frac{\hbar^2}{2M}\left[\frac{l(l+1)}{r^2}-\frac{d^2}{dr^2}\right], \quad (7)$$

M being the reduced mass of the incident particle. $E'=E-\epsilon$, where ϵ is the energy of the excited state.

For these nuclei of ground-state spin zero, $I=0$, $I'=2$, and $J=j=l\pm\frac{1}{2}$ only, where l is the orbital angular momentum in the entrance channel. In Eq. (5), $l'=l$, $l\pm2$, and $j'=l'\pm\frac{1}{2}$. Equation (6) represents five equations for each of $J=j=l\pm\frac{1}{2}$, corresponding to $l'=l$, $l\pm2$ and the allowed values of $j'=l'\pm\frac{1}{2}$, and the sum in Eq. (6) also goes over $l''=l$, $l\pm2$ and the allowed values of $j''=l''\pm\frac{1}{2}$. Hence, the wave equation separates into sets of six coupled equations, one set for each value of l and of $J=l\pm\frac{1}{2}$. We shall assume that only the scalar and quadrupole parts of the interaction are effective, and this leads immediately to the above restrictions on the l and j values. For incident partial waves $l=0$, 1, 2, some of these equations and parts of the sums drop out because of angular momentum coupling considerations. Hence, $l=0$, 1, 2 need to be treated as special cases.

Before the coupled equations (5) and (6) can be solved, it is necessary to evaluate the matrix elements $V_{I'j'l':Ijl}{}^J(r)$ of the interaction potential. We have

$$V_{I'j'l':Ijl}{}^J(r)=(\phi_{I'j'l'}{}^{JM}(\hat{r},\xi)\,|\,V(\mathbf{r},\xi)\,|\,\phi_{Ijl}{}^{JM}(\hat{r},\xi)). \quad (8)$$

The round brackets indicate integration over the nuclear coordinates ξ and the angular variables $\hat{r}$, but not over r. The interaction is written as a sum of products of multipole tensor operators,

$$V(\mathbf{r},\xi)=\sum_{Qq}Y_Q{}^{q*}(\hat{r})T_Q{}^q(r,\xi). \quad (9)$$

By using the definition of Eq. (4), we can soon evaluate Eq. (8) to give a calculable formula for the required potential matrix elements. We obtain

$$V_{I'j'l':Ijl}{}^{(Q)J}(r)=V_{II'}F_{II'}{}^{(Q)}(r)i^{l-l'}(-)^{J+1/2}(-)^{j+j'}\times[(2j+1)(2j'+1)(2l+1)(2l'+1)]^{1/2}\times C_{000}{}^{Ql'l}W(ljl'j':\tfrac{1}{2}Q)W(IjI'j':JQ), \quad (10)$$

where

$$V_{II'}{}^{(Q)}F_{II'}{}^{(Q)}(r)=\frac{(-)^I[2I'+1]^{1/2}\langle I'\|T_Q\|I\rangle}{(4\pi)^{1/2}}. \quad (11)$$

The quantity $\langle I'\|T_Q\|I\rangle$ is a reduced nuclear matrix element defined, by means of the Wigner-Eckart theorem, as follows:

$$(\Psi_{I'}{}^{k'}(\xi)\,|\,T_Q{}^q(r,\xi)\,|\,\Psi_I{}^k(\xi))=C_{k'qk}{}^{I'QI}\langle I'\|T_Q\|I\rangle. \quad (12)$$

It may be readily shown from these formulas that we have the symmetry relation,

$$V_{I'j'l':Ijl}{}^{(Q)J}(r)=V_{Ijl:I'j'l'}{}^{(Q)J*}(r). \quad (13)$$

The matrix elements of the scalar component of the interaction ($Q=0$) are taken to be the usual type of complex optical potentials employed in elastic scattering work. They are assumed to be independent of I and the same in both elastic and inelastic channels. We employ a real Saxon potential plus volume and surface absorptive terms, a Coulomb interaction due to a uniform spherical charge distribution, and a spin-orbit potential of the Thomas form. Hence,

$$V_{Q=0}=V_c(r)-V_S f_S(r)-iW_I f_I(r)-iW_D f_D(r)-V_{SO}\left(\frac{\hbar}{m_\pi c}\right)^2\left[-\frac{1}{r}\frac{df_S(r)}{dr}\right]\mathbf{l}\cdot\boldsymbol{\sigma}. \quad (14)$$

In this equation, V_S, W_I, and W_D are potential depths (i.e., positive numbers) and V_{SO} is also positive in agreement with the shell-model assignment. We have

$$f_S(r)=\left[1+\exp\left(\frac{r-R_S}{a_S}\right)\right]^{-1}, \qquad R_S=r_S A^{1/3}, \quad (15)$$

$$f_I(r)=\left[1+\exp\left(\frac{r-R_I}{a_I}\right)\right]^{-1}, \qquad R_I=r_I A^{1/3}, \quad (16)$$

$$f_D(r)=4\exp\left(\frac{r-R_D}{a_D}\right)\Big/\left[1+\exp\left(\frac{r-R_D}{a_D}\right)\right]^2, \qquad R_D=r_D A^{1/3}, \quad (17)$$

where A is the nuclear mass in atomic mass units. Since the results are not sensitive to the value of the charge radius R_c, within reasonable limits, we shall

set $R_c=R_S$. Hence,

$$V_c(r)=Z_IZ_Te^2/r, \qquad r\geqslant R_S,$$
$$=\frac{Z_IZ_Te^2}{2R_S}\left[3-\frac{r^2}{R_S{}^2}\right], \qquad r<R_S, \tag{18}$$

where Z_I, Z_T are the incident and nuclear charges. Also, for the scattering state symbolized by $|jl\rangle$,

$$\mathbf{l}\cdot\boldsymbol{\sigma}|jl\rangle=[j(j+1)-l(l+1)-\tfrac{3}{4}]|jl\rangle. \tag{19}$$

For the matrix elements of the quadrupole component of the interaction ($Q=2$) we use the expression in Eq. (10). Explicit formulas for the coupling strengths $V_{II'}{}^{(2)}$ and the form factors $F_{II'}{}^{(2)}(r)$ can be found only by employing definite nuclear models and using Eqs. (11) and (12). If, for instance, a single-particle excitation model is proposed, they may be calculated in terms of shell-model wave functions and assumed two-body forces. The collective rotation and quadrupole vibration models will be considered in detail in the next section.

However, on general theoretical grounds, the form factors $F_{02}{}^{(2)}(r)$ and $F_{22}{}^{(2)}(r)$ should be zero at $r=0$ and peaked inside or near the nuclear surface. In addition, for single-particle excitations, the form factors may have nodes in the nuclear interior. In the present calculation we chose a simple parametric form for the coupling functions which was peaked near the nuclear surface and left the strengths $V_{02}{}^{(2)}$ and $V_{22}{}^{(2)}$ as input numbers. We set

$$F_{02}{}^{(2)}(r)=F_{22}{}^{(2)}(r)$$
$$=\exp\left(\frac{r-R_F}{a_F}\right)\Big/\left[1+\exp\left(\frac{r-R_F}{a_F}\right)\right]^2,$$
$$R_F=r_FA^{1/3}. \tag{20}$$

Thus, various nuclear models could be simulated by varying the strength ratios and the two parameters of the coupling functions.

For incoming state $|jl\rangle$, we have, in general, six coupled equations. We integrate the coupled set six times numerically, each time using different initial values for the functions near the origin. The integrations are carried out to the nuclear surface where the optical and coupling potentials eventually become negligible. The six independent solutions for each of the six radial wave functions are then superposed to yield the true wave functions. The superposition coefficients are determined by setting up a 12×12 complex matrix equation which matches the internal nuclear functions and their derivatives to the corresponding incoming and outgoing free-state Coulomb wave functions.[3] Of course, we require outgoing Coulomb waves only for the inelastic scattering channels. The solution of the matrix equations yields automatically the elastic and inelastic scattering matrix elements, from which the corresponding cross sections are easily computed. This procedure is repeated for each partial wave l and for each $j=l\pm\frac{1}{2}$, up from $l=0$, until the scattering phase shifts are negligible.

The whole calculation was coded for the IBM 7090 at Oak Ridge. For incident protons, the code gives the total absorption cross section, the total inelastic 2^+ cross section, the elastic and inelastic differential cross sections, and the corresponding polarizations. For incident neutrons, we obtain also the total nuclear and total elastic cross sections.

A. Collective 2^+ States

In this section we evaluate the coupling functions by means of Eqs. (11) and (12), using the permanently deformed nucleus model[4] and the pure quadrupole vibration model.[5] These are, of course, extremely simplified representations of nuclear collective motions.

1. *The Rotational Model*[4]

Here we consider a nucleus characterized by a permanently deformed surface of cylindrical symmetry.

$$R(\theta\phi)=R_S[1+\beta Y_2{}^0(\theta\phi)], \tag{21}$$

that is,

$$R(\theta\phi)=R_S\left[1+\beta\left(\frac{4\pi}{5}\right)^{1/2}\sum_m Y_2{}^{m*}(\theta,\phi)Y_2{}^m(\hat{S})\right]. \tag{22}$$

The direction $\hat{S}$ specifies the orientation of the nuclear symmetry axis and β is the conventional nuclear deformation parameter. $\beta>0$ and $\beta<0$ refer, respectively, to prolate and oblate deformations. Assume that the potential seen by the incident particle depends only on its distance from the nuclear surface. Then

$$V\{r-R(\theta\phi)\}=V(r-R_S)$$
$$-\beta\left(\frac{4\pi}{5}\right)^{1/2}\sum_m Y_2{}^{m*}(\theta\phi)Y_2{}^m(\hat{S})\cdot R_S\frac{dV}{dr} \tag{23}$$

to first order in β. dV/dr is evaluated for $\beta=0$. For an interaction of the Saxon form, as in Eq. (15),

$$-V=V_Sf_S(x)+\frac{\beta R_SV_S}{a_S}\left(\frac{4\pi}{5}\right)^{1/2}g(x)$$
$$\times\sum_m Y_2{}^{m*}(\hat{r})Y_2{}^m(\hat{S}), \tag{24}$$

where $x=(r-R_S)/a_S$. $f_S(x)$ is defined in Eq. (15), and $g(x)=F_{II'}{}^{(2)}(x)$ is given by Eq. (20) if we set $R_F=R_S$ and $a_F=a_S$. Hence, by definition and use of

[3] B. Buck, R. N. Maddison, and P. E. Hodgson, Phil. Mag. **5**, 1181 (1960).

[4] A. Bohr and B. R. Mottelson, Kgl. Danske Videnskab. Selskab, Mat.-Fys. Medd. **27**, No. 16 (1953).

[5] A. Bohr, Kgl. Danske Videnskab. Selskab, Mat.-Fys. Medd. **26**, No. 14 (1952).

Eqs. (11) and (12), we have

$$V_{II'}{}^{(2)}=\frac{\beta R_S V_S}{a_S}\left[\frac{2I'+1}{5}\right]^{1/2}(-)^I \times\frac{(\Psi_{I'}{}^{k'}|\,Y_2{}^m(\hat{S})\,|\Psi_I{}^k)}{C_{k'mk}{}^{I'2I}}. \quad (25)$$

The nuclear wave functions for the ground-state rotational band can be written

$$\Psi_I{}^k=\left[\frac{2I+1}{8\pi^2}\right]^{1/2}D_{k0}{}^I(\hat{S}),$$
$$\Psi_{I'}{}^{k'}=\left[\frac{2I'+1}{8\pi^2}\right]^{1/2}D_{k'0}{}^{I'}(\hat{S}). \quad (26)$$

Also,

$$Y_2{}^m(\hat{S})=\left(\frac{5}{4\pi}\right)^{1/2}D_{m0}{}^2(\hat{S}), \quad (27)$$

where the D's are elements of the rotation matrix. Inserting Eqs. (26) and (27) into Eq. (25), we soon find

$$V_{II'}{}^{(2)}=\frac{\beta R_S V_S}{a_S(4\pi)^{1/2}}(-)^I[2I+1]^{1/2}C_{000}{}^{I'2I}. \quad (28)$$

Hence, the two coupling strengths $V_{02}{}^{(2)}$ and $V_{22}{}^{(2)}$ are

$$V_{02}{}^{(2)}=+\frac{\beta R_S V_S}{a_S(4\pi)^{1/2}},\quad V_{22}{}^{(2)}=-\left(\frac{10}{7}\right)^{1/2}V_{02}{}^{(2)}. \quad (29)$$

Thus, the coupling strengths can be calculated from the assumed deformation parameter β and the parameters of the optical potential, while the form factors are essentially the derivatives of the Saxon potential shape.

2. *The Vibrational Model*[5]

In this case, the nuclear surface is characterized by dynamical deformation parameters α_μ.

$$R(\theta\phi)=R_S[1+\textstyle\sum_\mu \alpha_\mu{}^* Y_2{}^{\mu*}(\theta\phi)]. \quad (30)$$

Again assuming that the potential felt by the incident particle depends only on its distance from the nuclear surface, we have, to first order,

$$-V=V_S f_S(x)+\frac{R_S V_S}{a_S}g(x)\sum_\mu \alpha_\mu{}^* Y_2{}^{\mu*}(\theta\phi) \quad (31)$$

where $x=(r-R_S)/a_S$. As before, $f_S(x)$ is defined by Eq. (15) and $g(x)=F_{II'}{}^{(2)}(x)$ is given by Eq. (20) when we set $R_F=R_S$ and $a_F=a_S$. In the usual way, α_μ is decomposed into operators b_μ and $b_\mu{}^*$ which, respectively, destroy and create a single quadrupole phonon of vibration.

$$\alpha_\mu=\left[\frac{\hbar\omega}{2C}\right]^{1/2}[b_\mu+(-)^\mu b_{-\mu}{}^*], \quad (32)$$

where

$$\alpha_\mu=(-)^\mu\alpha_{-\mu}{}^*. \quad (33)$$

Also,

$$b_\mu b_\mu{}^*=n_\mu+1,\quad b_\mu{}^* b_\mu=n_\mu,\quad \textstyle\sum_\mu n_\mu=N, \quad (34)$$

where N is the number of phonons in a state. The quadrupole phonon states are written as follows:

$$\Psi_I{}^k=|N{:}Ik\rangle,\quad \langle N{:}Ik|N{:}Ik\rangle=1. \quad (35)$$

$$\text{Vacuum state: } |0{:}00\rangle=|0\rangle,$$
$$\text{1-Phonon state: } |1{:}2k\rangle=b_k{}^*|0\rangle. \quad (36)$$

Analogously to the permanent deformation parameter β used in the last section, we introduce a dynamical or root mean square deformation parameter. The new β is defined so that β^2 is the expectation value of $\sum_\mu|\alpha_\mu|^2$ in the nuclear ground state.

$$\beta^2=\langle 0|\textstyle\sum_\mu|\alpha_\mu|^2|0\rangle. \quad (37)$$

Using Eqs. (32) and (34), we easily find that

$$\beta^2/5=\hbar\omega/2C. \quad (38)$$

Hence,

$$\alpha_\mu=(\beta/\sqrt{5})[b_\mu+(-)^\mu b_{-\mu}{}^*]. \quad (39)$$

By means of the definitions given earlier, we have

$$V_{II'}{}^{(2)}=\frac{\beta R_S V_S}{a_S(4\pi)^{1/2}}\left[\frac{2I'+1}{5}\right]^{1/2}(-)^I \times\frac{\langle N'{:}I'k'|\,b_\mu{}^*|\,N{:}Ik\rangle}{C_{k'\mu k}{}^{I'2I}}. \quad (40)$$

This is easily evaluated to yield

$$V_{02}{}^{(2)}=+\frac{\beta R_S V_S}{a_S(4\pi)^{1/2}},\quad V_{22}{}^{(2)}=0. \quad (41)$$

The diagonal strength $V_{22}{}^{(2)}$ of the quadrupole interaction vanishes because $b_\mu{}^*$ can only connect states which differ by one in the number of phonons. It is fairly straightforward to verify that when $V_{22}{}^{(2)}=0$, the results of the coupled channels calculations do not depend on the sign of β.

We see from the above derivations that, with suitable and natural definitions of the permanent or dynamical distortion parameters β, the two models give identical expressions for $V_{02}{}^{(2)}$. The models can only be distinguished if the presence or absence of the strength $V_{22}{}^{(2)}$ has large effects on the results of calculation. It turns out that the two models give very similar results for the energies and nuclear masses considered here. In Fig. 1 we illustrate this point by means of typical calculations of the inelastic 2^+ angular distribution of protons from the reaction $Fe^{56}(p,p')$ at 14.1 MeV. The geometrical parameters and spin-orbit potential are the same as in the standard set given in Table I, while V_S and W_D for this reaction are contained in Table II.

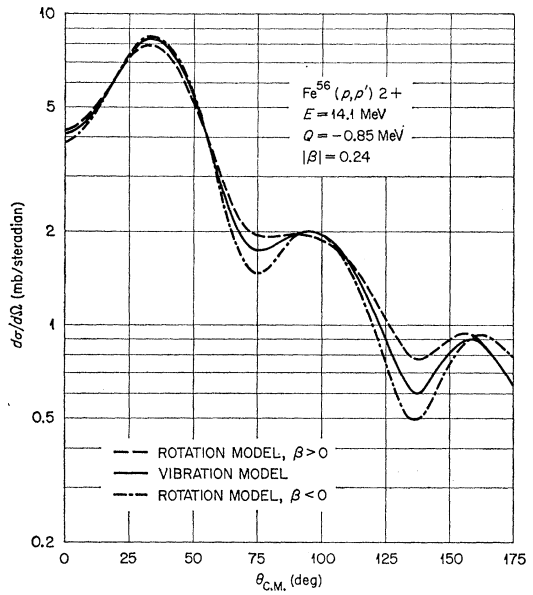

FIG. 1. Comparison of collective models. The three curves are theoretical results for the 2^+ inelastic scattering of protons from Fe^{56} at 14.1 MeV, using a prolate permanent deformation, an oblate deformation, and the vibrational or dynamical distortion model. The parameters employed are given in Tables I and II.

We chose $|\beta|=0.24$ and we give the results for the two cases $\beta>0$ and $\beta<0$ on the rotational model and the result for the vibration model where the sign of β is irrelevant. The curves show that while it may just be possible to distinguish experimentally between prolate and oblate deformations if the nucleus is permanently deformed, it would not be possible to distinguish between the vibrational model and either of the above two extreme cases.

B. Critique and Discussion

The calculations described above may be criticized on several grounds. First, it would be desirable to include explicitly the process of Coulomb excitation of the 2^+ state by the incident protons. This process interferes destructively with the purely nuclear excitation mechanism. The contribution of Coulomb excitation is, in principle, straightforward to calculate within the framework of the present treatment. One assumes that the charge distribution is deformed in the same way as the potential distribution. This leads to the introduction into the coupling form factors of additional terms proportional to r^{-3} when r is greater than the average charge radius R_c, and proportional to r^2 when $r<R_c$. The proportionality factors are soon calculated for a uniform, quadrupole distorted charge distribution. In practice, one would need to integrate the sets of coupled equations for a very large number of partial waves if the Coulomb excitation process was to be treated correctly. Fortunately, this excitation mechanism is expected to be negligible for the experiments considered in this paper.

Second, it may seem dangerous to neglect the effects of higher excited collective states, i.e., the 4^+, 6^+, etc., states of the rotational band or the 0^+, 2^+, 4^+ triplet of the vibrational nuclei. This is still an open question. However, a code has been written which couples together 0^+, 2^+, and 4^+ states, though spin-orbit coupling is neglected. Experience with this latter code indicates that the inclusion of the 4^+ state does not appreciably affect the elastic and inelastic scattering results provided that $\beta\leqslant 0.3$ approximately, and the energy is not too low. These conditions are not violated in the analyses presented later. More serious is the neglect of the 3^- octupole collective states which occur in a wide range of even-even nuclei and which are usually strongly excited by nucleon scattering. The effect of this on the other results remains to be investigated.

There is another ambiguity in the calculations. We have tacitly assumed that only the deformation of the real part of the optical potential is effective in coupling the elastic and inelastic channels. Naively, one might say that since the nucleus is deformed or deformable, then the absorptive potential should also be deformed or should undergo quadrupole vibrations. This would lead to imaginary terms in the coupling potentials evaluated earlier. But, equally naively, one could say that the absorption potential is introduced only to take care of all reaction processes *other than* the ones

TABLE I. Standard set: fixed optical potential parameters used in the final analysis described in Sec. 3B. See text for definition of symbols. Use of this model allows easy comparison of derived potential depth parameters V_S, W_D and nuclear deformabilities β with the results of other work.

r_S (F)	a_S (F)	r_D (F)	a_D (F)	r_F (F)	a_F (F)	V_{SO} (MeV)
1.25	0.65	1.25	0.47	1.25	0.65	8.0

TABLE II. Results provided by the search code. The geometrical parameters of the model and the spin-orbit magnitude were fixed at the values given in Table I. See text for the sources of the experimental measurements.

Nucleus	E (MeV)	V_S (MeV)	W_D (MeV)	β	σ_A (mb)	σ_{in}^{2+} (mb)
Ti	12.2	48.1	9.7	0.25	904.6	40.8
Cr	12.0	50.2	10.8	0.20	904.0	23.8
Ni	12.0	48.4	9.1	0.28	881.6	54.9
Zn	11.9	50.0	10.6	0.24	919.7	42.3
Ti	14.3	47.4	11.0	0.26	970.2	34.7
Cr	14.3	49.6	12.2	0.19	983.1	19.2
Fe	14.1	48.2	11.6	0.24	979.8	33.6
Ni	14.3	48.5	9.7	0.23	954.4	40.7
Zn	14.3	49.0	11.8	0.23	1001.0	35.5
Ni	15.0	48.2	10.3	0.22	974.6	35.9
Ni	16.8	48.4	9.7	0.20	989.2	34.5
Fe	17.3	47.6	10.0	0.21	1007.0	33.2
Ni	17.3	47.5	9.1	0.20[a]	981.6	35.7
Zn	17.3	48.2	10.5	0.23[a]	1047.0	43.3

[a] β fixed: only elastic distributions available.

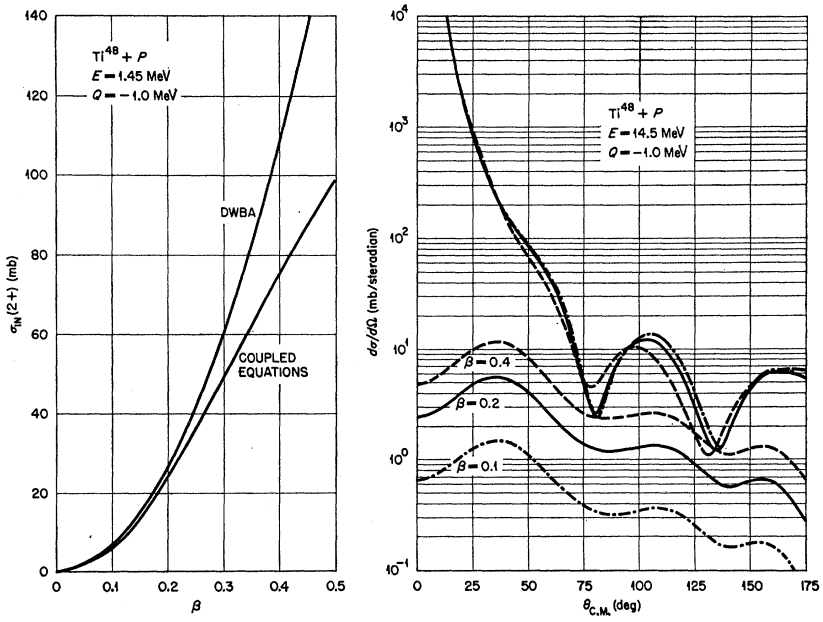

FIG. 2. Comparison of the present theory with the distorted-wave Born approximation for $Ti^{48}(p,p')$ at 14.5 MeV. The parameters used in the calculations are obtained from Table I, and Eqs. (45) and (46).

treated explicitly by means of coupled channels and, therefore, it should not contribute to these latter reactions. In any case, even if the coupling potentials should be complex, it is not at all evident what form the imaginary parts should have. Again the matter remains to be investigated; but it does not appear to be very important when one considers the other uncertainties in the models employed. A similar ambiguity afflicts the introduction of the spin-orbit potential. Perhaps one should make this deformed too and so have a source of spin-flip processes. This is felt to be important only for the calculation of the inelastic polarization.

Apart from the uncertainties mentioned above, there is yet another fundamental dilemma in the treatment of the diffuse-edged collective model for inelastic scattering. An alternative prescription states that instead of defining the deformed potential as in Eq. (23) [or as in Eq. (31), if we are considering the vibration model] one should use the expression, $V\{r(\theta\phi)-R_S\}$, where $r(\theta\phi)=r[1-\beta Y_2^0(\theta\phi)]$, r being the radial coordinate of the incident particle. The expansion to first order in β leads again to our formulas, except that the coupling form factors should be multiplied by r/R_S. This modification should not lead to appreciably different results for the case of proton scattering.

Finally, all the optical and coupling interactions should, presumably, be nonlocal operators in coordinate space. Modern theories for the interaction of nucleons and nuclei always give rise to some form of nonlocality. Usually, we can take this into account by allowing the optical potentials to be energy dependent. A more detailed consideration of nonlocal effects in the strong coupling theory of inelastic scattering would present serious computational difficulties.

We now discuss some general properties of coupled channel calculations. First, it may be noted that if the sum of coupling terms in Eq. (5) is neglected, the whole calculation is mathematically equivalent to the distorted-wave Born approximation (DWBA) theory of direct interaction inelastic scattering. This theory is usually presented so that the inelastic scattering cross section appears as the square modulus of a perturbation theory matrix element. Schematically,

$$\frac{d\sigma(2+)}{d\Omega}\propto\beta^2|\langle\Psi_f^{(-)}|F(r)Y_2^0(\hat{r})|\Psi_i^{(+)}\rangle|^2. \quad (42)$$

Here, β is the deformation parameter and $F(r)$ is an interaction form factor similar to those mentioned earlier. $\Psi_i^{(+)}$ and $\Psi_f^{(-)}$ are essentially initial and final elastic scattering wave functions calculated with a spherical optical model.

We see that the cross-section magnitude is always proportional to β^2 and that the angular distribution shape is independent of β. Figure 2 contains a comparison between the DWBA theory and the present calculation for the elastic and inelastic scattering of protons from Ti^{48} at 14.5 MeV. This case is typical of those analyzed later. The first diagram shows a plot of the total inelastic 2^+ cross section as a function of β. For $\beta\leqslant 0.1$, the two theories give essentially identical results and $\sigma_{IN}(2+)\propto\beta^2$. But when $\beta\gtrsim 0.1$, there is a marked divergence and, for a given β, the DWBA overestimates the cross section considerably, e.g., by $\sim 10\%$ at $\beta=0.2$ and by $\sim 20\%$ at $\beta=0.3$. It is interesting to see that from $\beta=0.2$ to $\beta=0.4$, $\sigma_{IN}(2+)\propto\beta$ in the present theory, not β^2 as in DWBA. Similar results were obtained from calculations on Fe and Zn. The results on Ti, Fe, and Zn, taken together, indicated that,

for a fixed value of β, the theoretical total 2^+ cross sections were proportional to the nuclear mass A.

The second diagram shows the elastic and inelastic angular distributions as functions of β. The DWBA treatment would give elastic and inelastic distribution shapes close to those labeled $\beta=0.1$. We see that as β is increased the inelastic differential cross section grows in magnitude, though not as fast as in DWBA, and its shape does not change appreciably. Hence, DWBA is probably adequate for calculating the inelastic cross section shapes, but not their magnitudes.

In DWBA, the elastic differential cross section is independent of β. But we find that strong channel coupling does have a large effect on the calculated elastic scattering. Hence, it is clear that if the elastic data, for instance, fell along the curve marked $\beta=0.1$, and if the inelastic magnitude demanded $\beta=0.4$, then one would need to change the optical-model parameters if one wished to fit elastic and inelastic differential cross sections simultaneously. This illustrates a general rule that when collective states are strongly excited the optical-model parameters obtained by fitting the elastic data with a spherical optical model are not necessarily the same as those found using the present model to fit elastic and inelastic data at the same time. The difference between spherical optical-model parameters and the deformed-nucleus model parameters becomes more marked as the incident particle energy decreases. A more detailed discussion of these effects is found in reference 1. As a final remark, we should say that inclusion of the 3^- octupole states in the calculation would require further adjustment of the potential depth values in order to fit all the data.

3. ANALYSIS OF PROTON SCATTERING

In this section we use the model to analyze proton elastic and 2^+ inelastic differential cross-section measurements. The data are taken from several sources and include experiments on natural targets of Ti, Cr, Fe, Ni, and Zn at energies between 12 and 17 MeV. The measurements at 12 and 14.3 MeV on Ti, Cr, Ni, and Zn were the work of Hu *et al.*[6] The Fe data at 14.1 MeV are due to Kikuchi *et al.*,[7] and the Ni data at 15 and 16.8 MeV were taken by Daehnick and Hill.[8] The elastic angular distributions for Fe, Ni, and Zn at 17.3 MeV are the work of Dayton and Schrank,[9] while the only inelastic distribution at this energy, that for Fe, was reported by Schrank *et al.*[10]

The analysis was greatly facilitated by attaching to the code described above an automatic parameter-searching routine. The search code adjusts the parameters of the model until the quantity

$$\chi^2=\sum_\theta \left\{\frac{\sigma_E(\theta)-\sigma_T(\theta)}{\Delta\sigma_E(\theta)}\right\}^2 \tag{43}$$

is a minimum. The suffices E and T refer, respectively, to the experimental and theoretical results. Both elastic and inelastic distributions are included in the sum over angles and thus the two differential cross sections are fitted simultaneously. The code was arranged so that up to 14 parameters could be varied automatically in the same run. For obvious practical reasons, this full generality was never used. We shall not quote the individual values of χ^2 obtained for the results given later, since these would only have meaning if we gave also the number of data points and the errors attached to each measurement. In a fairly typical case we have about 20 data points for each of the elastic and inelastic cross sections, while the quoted errors for the elastic scattering are of order 5% and the inelastic errors are of order 10%. For such cases we obtain values of the total χ^2 ranging from 100 to 400. Usually, about one third of the total χ^2 is contributed by the elastic results and the rest by the inelastic fitting. Nearly always we arrive at an excellent fit for the elastic cross section and results for the inelastic scattering which range from fair to good.

It was decided early to use an optical model with surface absorption only; hence in all the follows we set $W_I=0$. As discussed in reference 1, this is probably a good assumption for the incident energies considered here. All the nuclei mentioned above are thought to be, at least approximately, of the vibrational type. Thus, we shall always put the coupling strength $V_{22}^{(2)}=0$. The reason for this is indicated in the last section. Any breakdown of the vibrational model would lead to a nonzero value for $V_{22}^{(2)}$; but, as we have already illustrated, it is difficult to distinguish the presence or absence of this type of coupling. It would also be desirable to fix the geometrical parameters of the calculation so that systematics in the potential depth parameters and the deformabilities β will show up clearly. This was done only after the preliminary analysis presented below.

Again, we have seen that the vibrational model of the last section specifies that the parameters r_F, a_F of the collective coupling form factor should be set equal to the corresponding parameters r_S, a_S of the real Saxon optical potential. We did not employ this constraint in the preliminary calculations since we wished to use the experimental data to provide a clear-cut test of the suitability of the collective model. At this stage, therefore, the model was defined by the following ten parameters: V_S, r_S, a_S; W_D, r_D, a_D; β, r_F, a_F and V_{SO}. The coupling strength $V_{02}^{(2)}$ was calculated by means of Eq. (41). Since β is a free parameter, this does not imply any specialization to the collective model. To

[6] C. Hu, K. Kikuchi, S. Kobayashi, K. Matsuda, Y. Nagahara, Y. Oda, N. Takano, M. Takeda, and T. Yamazaki, J. Phys. Soc. Japan **14**, 861 (1959).
[7] K. Kikuchi, S. Kobayashi, and K. Matsuda, J. Phys. Soc. Japan **14**, 121 (1959).
[8] W. Daehnick and H. A. Hill (unpublished).
[9] I. E. Dayton and G. Schrank, Phys. Rev. **101**, 1358 (1956).
[10] G. Schrank, P. C. Gugelot, and I. E. Dayton, Phys. Rev. **96**, 1156 (1954).

sum up, the idea behind the preliminary work was to determine suitable fixed geometrical parameters (and spin-orbit strength) for use in later systematic calculations and to test the applicability of the simple vibrational nucleus considerations.

A. Validity of the Collective Model

The data referred to above contained eleven cases suitable for inclusion in the first survey. These were elastic and inelastic scattering measurements on Ti, Cr, and Zn at 12 and 14.3 MeV, on Ni at 14.3, 15, and 16.8 MeV, and on Fe at 14.1 and 17.3 MeV. The Ni data at 12 MeV were not used for reasons explained later, while inelastic data were not available for Ni and Zn at 17.3 MeV. We thus have a large enough number of typical experiments for us to be able to draw some general conclusions.

A series of searches on the data was run in which all ten parameters of the model were allowed to vary. A fairly well defined minimum for χ^2 was found in each case, and the final values for χ^2 were all in the lower part of the range mentioned earlier. The model parameters thus obtained varied erratically from case to case, as is to be expected in this type of procedure. Table III contains the average values of geometrical and spin-orbit parameters determined by this method. The individual results for the parameters r_S, a_S, and r_D do not, in most cases, depart from the averages by more than about 5%, while the departures for a_D were of order 15%. The particular values for the parameters r_F, a_F deviate from the quoted averages by about 10% and 20%, respectively. Hence, Table III represents a fairly reliable guide to an underlying average nuclear model. The cross-section calculations are not very sensitive, within reasonable limits, to the magnitude of the spin-orbit potential and we can tolerate departures from the tabulated average value of about 30%. Thus, we may use in later calculations any fixed reasonable value for V_{SO} in the range 5 to 10 MeV. Polarization data may help to remove this ambiguity.

The really striking result obtained here was that the average values for the coupling function parameters r_F, a_F were nearly the same as the corresponding average parameters r_S, a_S of the real part of the optical potential. The closeness of the agreement was quite unexpected, and is a strong indication of the validity of the collective model treatment of this type of inelastic nucleon reaction. In particular, the simple vibrational model prescriptions given earlier seem to work surprisingly well. Further support for the validity of the model will be presented below when we compare the values of β found in this work with those obtained by electromagnetic methods.

TABLE III. Model parameters obtained by averaging the results of the preliminary investigations described in Sec. 3A. Note that $r_F \approx r_S$ and $a_F \approx a_S$.

r_S (F)	a_S (F)	r_D (F)	a_D (F)	r_F (F)	a_F (F)	V_{SO} (MeV)
1.21	0.66	1.26	0.51	1.20	0.65	7.5

We have now justified the use of the collective model and derived one possible set of potential parameters for application to all cases. To test this, we fixed the model parameters of Table III at the given values and fitted all the data again. Only the quantities V_S, W_D, and β were allowed to vary in the search routine. The results obtained were only slightly worse than those found earlier when all the parameters were allowed to vary. The fits obtained were very similar to those given in the next section. It is useful to be able to fix so many parameters, for then we can study the possible systematic variations of the potential depths V_S and W_D and the deformabilities β. It turns out that these quantities also can be assigned suitable values within narrow limits.

B. Results of Calculation

Table I contains another possible set of fixed values for the geometrical parameters of the model and for the spin-orbit potential depth. These parameter values are very close to the corresponding numbers of Table III and we have used the above justification of the collective model to set $r_F = r_S$ and $a_F = a_S$. The quality of fits obtained by use of Table I is essentially the same as found when Table III is employed. Several considerations indicate the use of the second set of fixed parameters in the final analysis rather than the first set; but most important is that this choice allows easy comparison of the results with the conclusions of similar and related work.

First, it is clearly desirable that the parameters for neutron and proton scattering should be closely the same. Hence, we employ as a guide the values given by Bjorklund and Fernbach,[11] which they derived from an analysis of medium energy neutron elastic scattering. Their treatment contained a Gaussian surface absorption, while ours uses one of the Saxon derivative type [see Eq. (17)]. Thus, our absorptive diffuseness a_D has to be chosen to correspond with their Gaussian diffuseness. Second, essentially the same set of local potential geometrical parameters has been found to generate results equivalent to those predicted by the nonlocal model of Perey and Buck,[12] which gave a unified account of a wide range of neutron-scattering data. Finally, this set, quoted below as the standard model of Table I does indeed give a good basis for the calculation of proton elastic scattering over a larger range of energies and masses than we consider here. The broad survey of available elastic data is reported and discussed by Perey.[1]

Hence, to fit the available data we used the standard set (Table I) and allowed only V_S, W_D, and β to be

[11] F. Bjorklund and S. Fernbach, Phys. Rev. **109**, 1295 (1958).
[12] F. Perey and B. Buck, Nucl. Phys. **32**, 353 (1962).

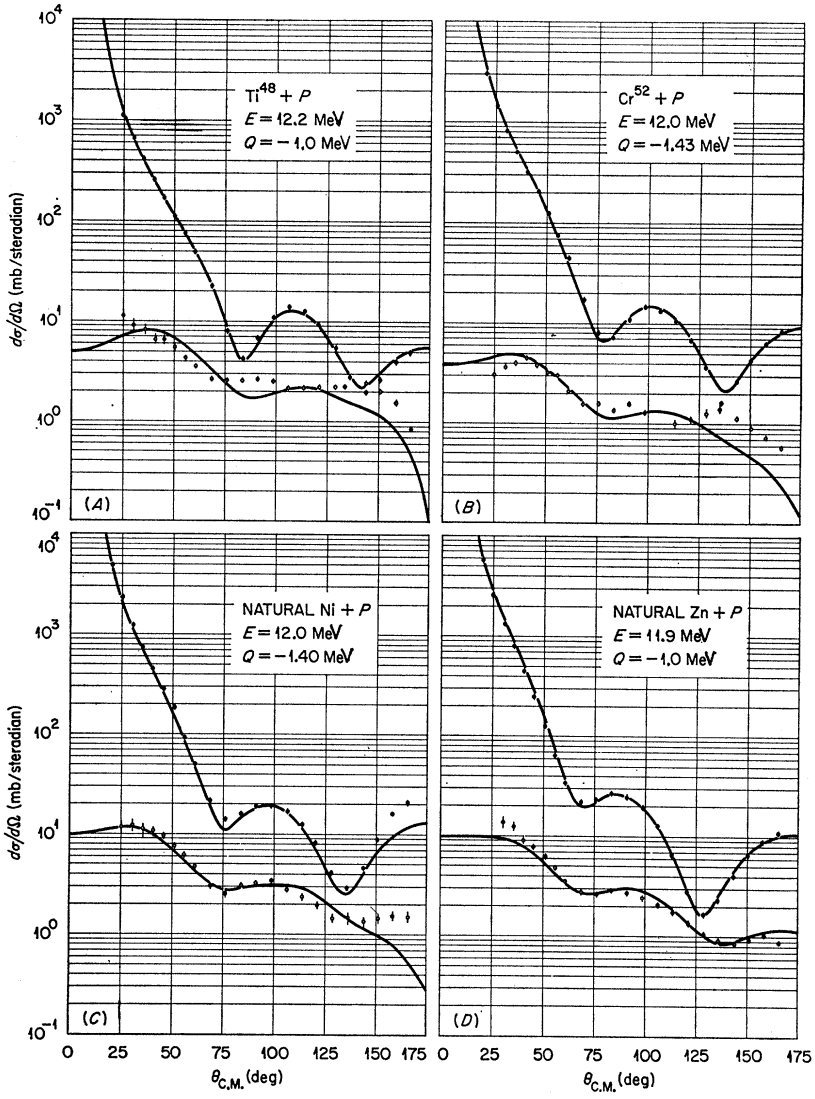

FIG. 3. Experimental and theoretical results at 12 MeV. The fixed model parameters are given in Table I and the final results for the varied quantities are in Table II.

adjusted by the search code. Of course, the magnitudes of V_S and W_D, corresponding to the two fixed models of Tables I and III, were different; but they showed the same general behavior as functions of mass and energy. It was very encouraging that the derived values of β for each nucleus, corresponding to the two models, differed only by a few percent. This suggests that, in conjunction with reasonable optical parameters and the collective considerations of the last section, model-independent values of the nuclear deformabilities β can be extracted from the inelastic proton scattering data.

The results are presented in the form of diagrams and a table. Figure 3 summarizes the experimental data and the theoretical calculations for 12-MeV incident proton energy. Figure 4 contains the 14-MeV results and Fig. 5 the available results at 17 MeV. Table II is a compendium of the final parameters obtained and contains the individual values for V_S, W_D, and β, together with the predicted results for the total inelastic 2^+ cross section and the total absorption cross section σ_A (which includes the contribution of $\sigma_{\text{in}}[2^+]$). The polarization results are not given. The elastic polarization predictions are very stable as functions of A and E and are essentially as given by Perey.[1] The inelastic polarizations vary quite appreciably with A and E; but no data are available for comparison. In addition, there are uncertainties in the calculation of the inelastic polarizations because we have not included the possibility of spin-flip processes.

C. Discussion of Results

In general, it will be seen from the diagrams that the elastic angular distributions are fitted remarkably well. However, the Ni results at 12 MeV do not quite reproduce the cross-section rise at angles greater than 140°. The reason for this will appear later. Also, there are marked discrepancies at forward angles in the

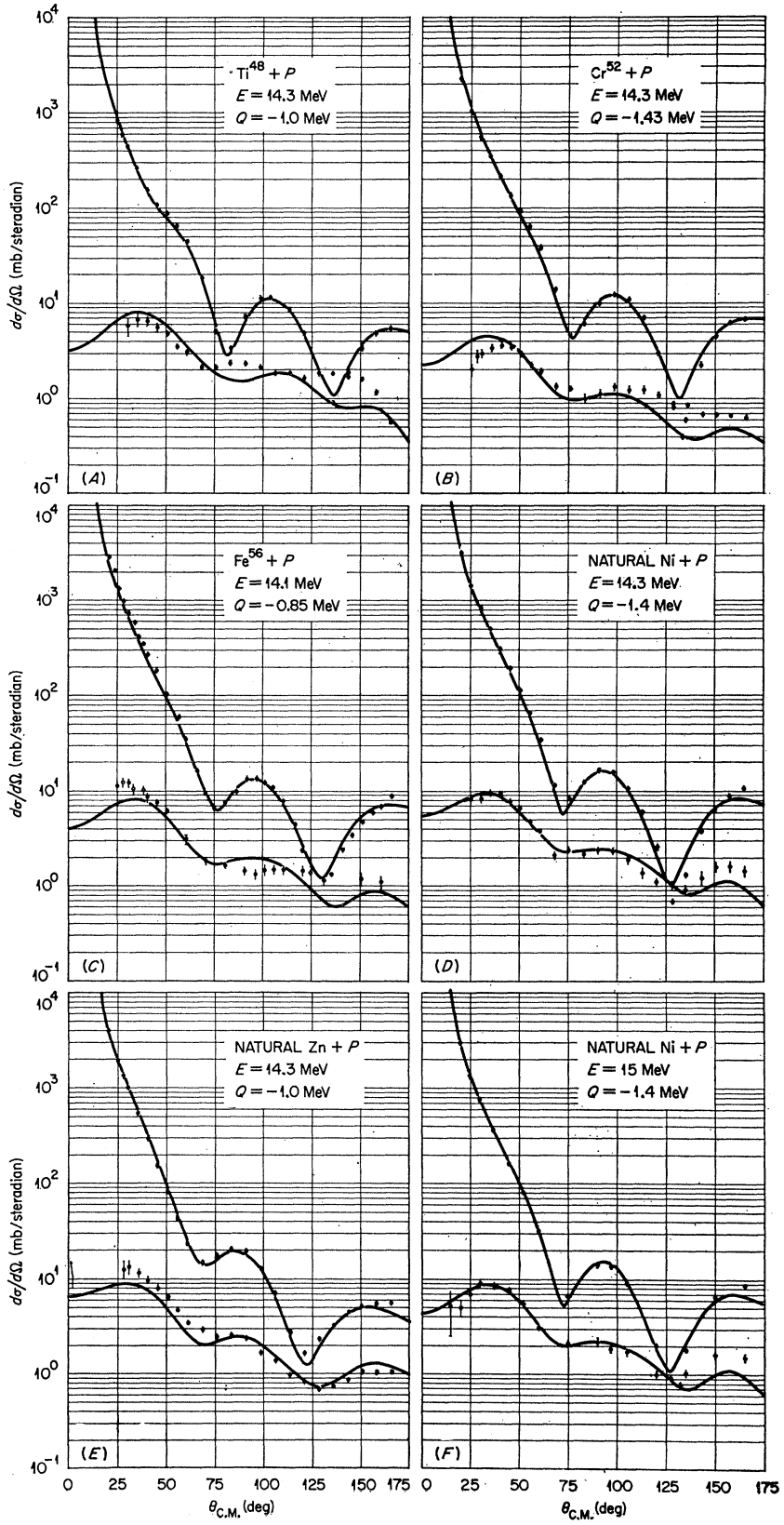

FIG. 4. Comparison of theory and experiment at 14–15 MeV. The fixed model parameters are given in Table I and the final results for the varied quantities are in Table II.

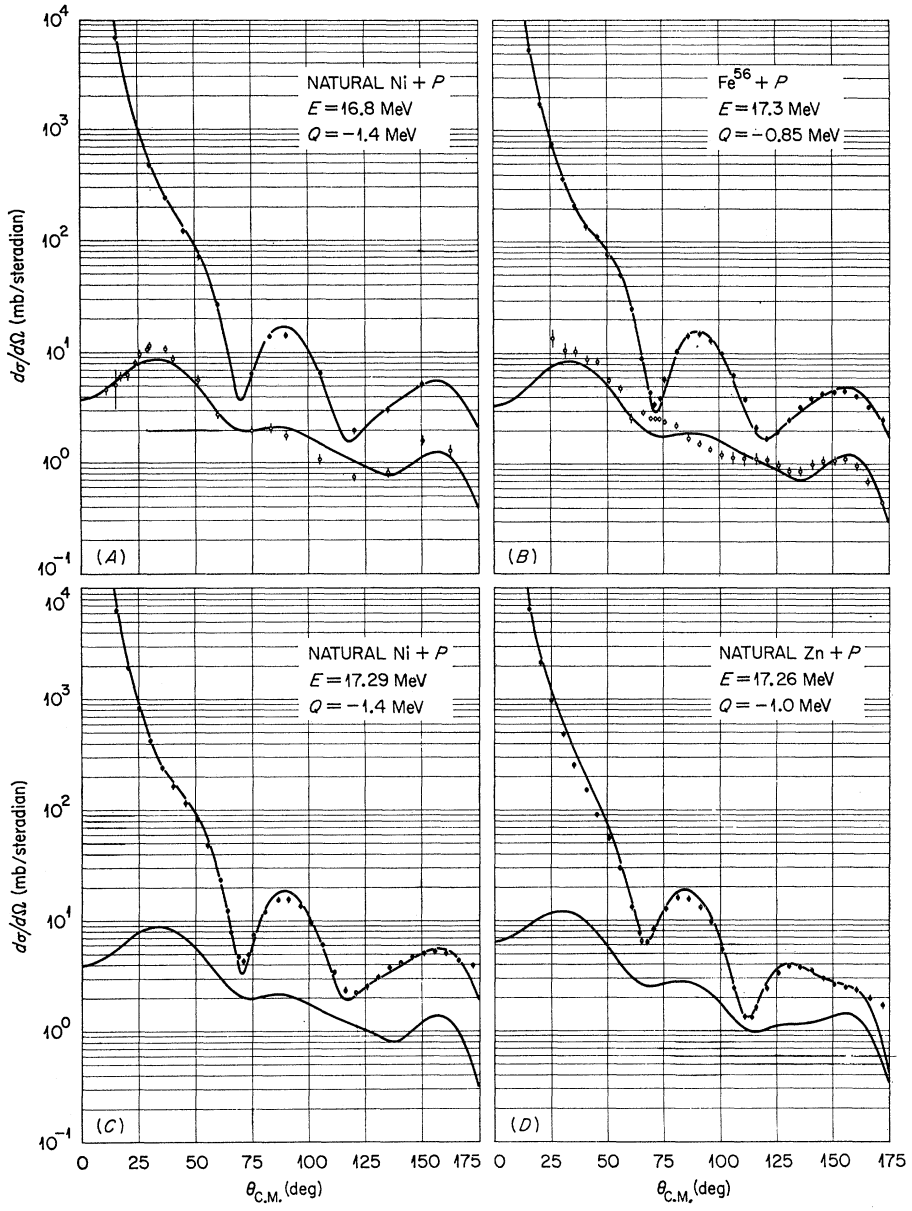

FIG. 5. Comparison of theory and experiment at 16.8–17.3 MeV. The fixed model parameters are given in Table I and the final results for the varied quantities are in Table II.

results for Fe at 14.1 MeV and Zn at 17.3 MeV. The cause of these disagreements is not known. The inelastic differential cross sections are fitted reasonably well in all cases and sometimes very well. The derived values of β are not expected to be very reliable when there is an appreciable difference of structure between experimental and theoretical distribution shapes. On the whole, the experimental inelastic data are much poorer than the elastic data, due to the technical difficulty of the experiments. The inelastic results on Ti and Cr at 12 and 14.3 MeV show only qualitatively good agreement with experiment. The calculations for Fe, Ni, and Zn at all energies are considerably better when compared with experiment, the Zn results being particularly successful.

In Fig. 6 the real potential well depth V_S and the surface absorptive well-depth W_D are plotted as functions of energy. Since only a few nuclei are considered, no useful conclusions can be drawn about the fluctuations of the potential values at a given energy. The results for the real potential V_S all lie within the indicated band shown in the diagram. There is an obvious tendency for V_S to decrease with energy. The nonlocal potential model[12] for the scattering of neutrons by nuclei indicated that, if one determined the local potential parameters equivalent to the nonlocal model

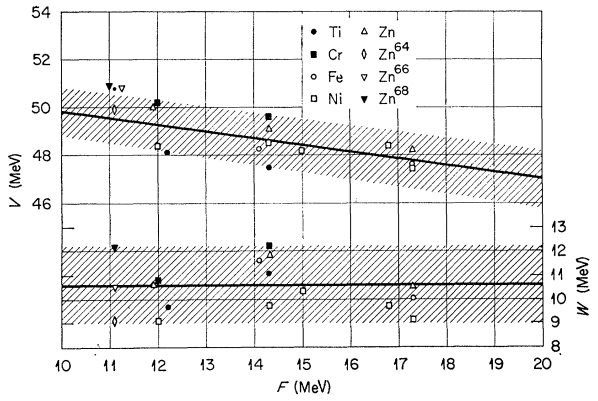

FIG. 6. Potential depth parameters obtained from the fitting of the data presented in Figs. 3, 4, and 5, plotted against the incident proton energy. The lines on the diagram indicate the average trends of the results.

at each energy, then over the energy range 0 to 20 MeV the neutron well depth varied linearly as a function of energy. The results for the neutron case could be summarized by the formula

$$V_S(n) \approx (48-0.29E) \text{ MeV}. \tag{44}$$

In the present case, where the geometrical and spin-orbit parameters are the same as in the neutron analysis, we can draw an average line through the indicated proton potentials. This line is shown on the diagram and the proton results can be represented by the equation

$$V_S(p) = (52.6-0.28E) \pm 1.0 \text{ MeV}. \tag{45}$$

Thus, the slope of line is nearly the same as for neutrons while zero-energy potential depth for protons is from 3.5 to 5.5 MeV deeper than the corresponding neutron depth. The origin of this increase is still rather obscure. To sum up, this analysis fixes the real potential well depth for protons to an accuracy of about 2%, indicates that it decreases linearly with energy and reveals that it is definitely larger than the neutron well depth at each energy.

The analysis of neutron scattering showed that the surface absorption potential magnitude was about 11 MeV and that it did not vary much with energy or mass number. The proton analysis given here indicates some considerable fluctuations; but the over-all results can be represented by the expression

$$W_D = 10.6 \pm 1.6 \text{ MeV} \tag{46}$$

at all energies and mass numbers. Hence, the surface-absorptive potential depth is only fixed within limits of $\pm 15\%$.

It is interesting to compare the values of the nuclear deformabilities β derived from the inelastic scattering experiments with the results determined by electromagnetic methods. The $B(E2)$ values for these nuclei, as extracted from Coulomb excitation and lifetime measurements, are taken from the forthcoming compilation prepared by Stelson.[13] To evaluate the electromagnetic β we assume a uniform nuclear charge distribution with a sharp surface of average radius $R_c = 1.2A^{1/3}$ F. For these dynamically deformable nuclei, the charge distribution has a root mean square effective quadrupole distortion. A first-order calculation leads to the following expression for β^2:

$$\beta^2 = \frac{B(E2:0 \rightarrow 2)}{[(3/4\pi)ZeR_c^2]^2}. \tag{47}$$

Taking the calculation to second order would yield slightly smaller values for β. When we consider the crudity of the model and the errors of the $B(E2)$ measurements, we estimate that Eq. (47) should give results for β within about 15% of the true values.

From the proton experiments on Ti we find that β lies between 0.25 and 0.26. though high quality fits to the angular distributions are not obtained. The $B(E2)$ result is $\beta \approx 0.26$. In Cr the inelastic proton scattering indicates that β is between 0.19 and 0.20, while the $B(E2)$ measurement implies $\beta \approx 0.23$. This seems to be a definite discrepancy; but again we observe that the shape fitting is not very good. The electromagnetic value for Fe is $\beta \approx 0.24$. We find two differing values from the inelastic data, i.e., $\beta = 0.24$ at 14.3 MeV and $\beta = 0.21$ at 17.3 MeV. In both cases the angular distributions agree reasonably well with the experimental data. Natural Zn appears to be a good case for comparison. Coulomb excitation measurements on the dominant isotopes Zn^{64}, Zn^{66}, and Zn^{68} indicate the values $\beta \approx 0.25$, 0.23, and 0.21, respectively. Taking into account the isotopic abundances in natural Zn (very approximately 50% Zn^{64}, 30% Zn^{66}, and 20% Zn^{68}) a reasonable average electromagnetic value is $\beta \approx 0.24$. This is consistent with the magnitudes derived from the inelastic data on natural Zn which lie between $\beta = 0.23$ and $\beta = 0.24$. It is obvious from the above discussion that only rather rough comparisons can be made between the deformabilities determined by electromagnetic and inelastic scattering methods. But it is fair to say that the β magnitudes obtained from the two techniques are in satisfactory agreement and this gives additional support to our collective model treatment of these reactions.

Natural Ni has been left for separate consideration since the derived values of β seem to vary strongly with energy: $\beta = 0.28$ at 12 MeV, $\beta = 0.23$ at 14.3 MeV, and $\beta = 0.20$ at 16.8 MeV. The Coulomb excitation value is $\beta \approx 0.20$. We meet here a phenomenon which greatly complicates work of this type at low proton energies. The quantity of interest in this connection is the (p,n) threshold energy for each nucleus. When the incident proton energy is below or only just above the (p,n) threshold then, if a compound nucleus is formed, one of the main channels for compound nuclear decay (i.e.,

[13] P. H. Stelson (private communication) and (to be published).

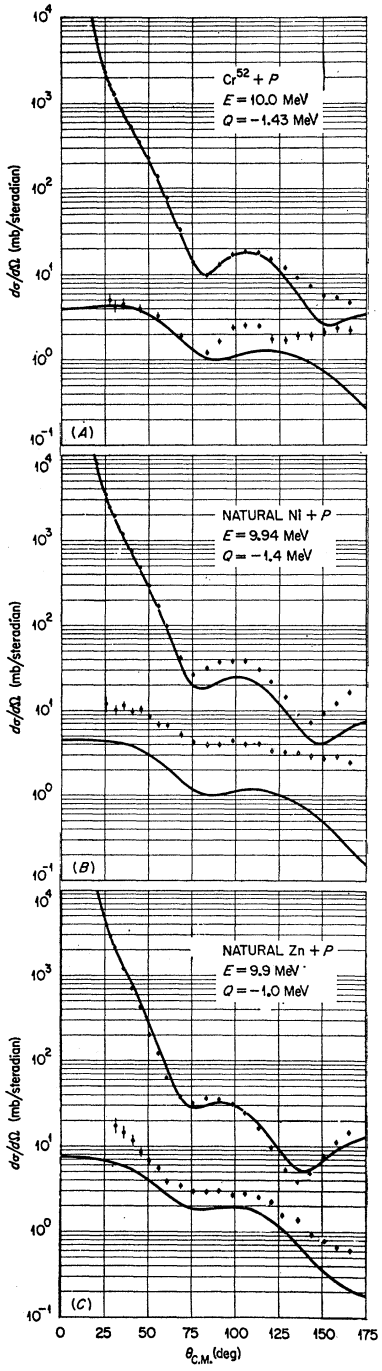

FIG. 7. Experimental and theoretical results at 10 MeV. Model parameters were fixed from Table I and Eqs. (45) and (46). See text for interpretation of the results.

neutron emission) is greatly inhibited. Since there is not a large number of target nuclear levels below the (p,n) threshold, the compound nucleus will have an appreciable branching ratio for decaying by proton emission to the ground state and low-lying levels of the target nucleus. Hence, we get compound elastic and inelastic proton reactions. Ni provides a good example of this, because the (p,n) threshold is approximately 9 MeV. In practice, it turns out that one needs to be about 5 MeV above the neutron threshold before compound scattering effects can be neglected. Hence for Ti, Cr, Fe, and Zn the effect can be ignored at energies greater than 12 MeV. But for Ni, the incident proton energy must be greater than 14 MeV before we can safely use direct reaction theory alone. Thus, we interpret the apparent rapid increase of β, as the energy is lowered, as due to the large contributions of compound nucleus processes to both elastic and inelastic proton scattering.

To illustrate this point further we calculate the elastic and inelastic cross sections for Cr, Ni, and Zn at $E\approx 10$ MeV and compare the results with the corresponding data of Hu *et al.* The (p,n) thresholds for these nuclei are 5.5, 9.3, and 7.8 MeV, respectively, so that at $E\approx 10$ MeV we expect some compound contamination in all three cases; least for Cr and most for Ni. Zn is an intermediate example. We fixed V_S from Eq. (45) to be 49.8 MeV and set $W_D=10.6$ MeV. The β values for Cr, Ni, and Zn were taken to be 0.20, 0.20, and 0.24, respectively, as indicated by the higher energy data. Comparison of theory and experiment in Fig. 7 bears out the interpretation fairly well. Some compound contribution is evident for Cr. For Zn there is already a fairly sizeable amount of compound inelastic scattering at 10 MeV. Finally, the Ni results indicate large contributions of compound nucleus processes to both elastic and inelastic scattering cross sections.

It is difficult to calculate the contributions of the compound nuclear reactions. The most obvious method is to use the statistical nucleus assumption for the compound processes and so reduce the calculation to the Hauser-Feshbach model[14] as modified for incident protons and emitted nucleons. But in order to do this one must know the spins, parities, and energies of all excited levels in the relevant nuclei below the incident proton energy. Information on these quantities for the required range of excitation energies is scarce and unreliable.

D. Separated Isotopes

From the viewpoint of this analysis, a very interesting kind of experiment is to measure the elastic and inelastic differential cross sections for the separated isotopes of an element. Such measurements are now becoming available. Here we consider the data of Beurtey *et al.*[15] on the separated isotopes Zn^{64}, Zn^{66}, and Zn^{68} at 11.1 MeV. Using the standard parameters of Table I and searching on the data as before yielded the results shown in Fig. 8. All the measured differential cross sections are fitted remarkably well. Very low values of χ^2 were obtained and the final numerical results for the automatically varied parameters V_S, W_D, and β are given in Table IV.

We see that the values of W_D all lie within the range

[14] W. Hauser and H. Feshbach, Phys. Rev. **87**, 366 (1952).
[15] R. Beurtey, P. Catillon, R. Chaminade, H. Faraggi, A. Papineau, and J. Thirion, Nucl. Phys. **13**, 397 (1959).

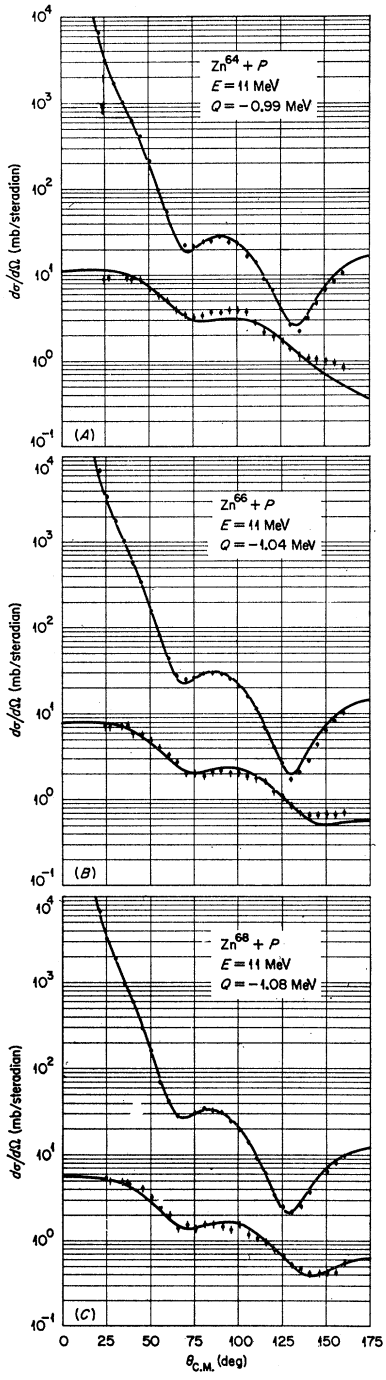

FIG. 8. Comparison of theory and experiment for the separated isotopes of Zn at 11.1 MeV. The fixed parameters are in Table I, final results for varied quantities in Table IV.

implied by Eq. (46); in fact, the result for Zn^{66} is the average value while the results for Zn^{64} and Zn^{68} appear at the extremes of the range. For 11.1 MeV, Eq. (45) predicts a real potential well-depth of $V_S=49.5\pm1$ MeV. The value obtained for Zn^{64} is within this range while the other values are just outside it. In this type of experiment, where the incident proton energy and the Z numbers of the targets are fixed, the main source of potential parameter fluctuations may be a symmetry energy contribution proportional to $(N-Z)/A$. In the case given here it is easily verified that the values obtained for W_D show a correlation of this type, while the results for V_S are erratic. Again, no definite conclusions can be drawn from results on such a limited range of nuclei.

The values of β derived from the fitting of these experiments may be compared directly with the magnitudes obtained by electromagnetic methods. The $B(E2)$ measurements give $\beta\approx0.25$ for Zn^{64}, $\beta\approx0.23$ for Zn^{66}, and $\beta\approx0.21$ for Zn^{68}. The corresponding results from the inelastic proton scattering data are $\beta=0.27$, $\beta=0.23$, and $\beta=0.20$. Thus, the two techniques yield deformability parameters in very satisfactory agreement with each other. The inelastic result for Zn^{64} seems to be a little high; but it should be recalled that this nucleus has a (p,n) threshold energy of 7.8 MeV, so that at 11.1-MeV incident proton energy we should expect a little compound nucleus contamination.

TABLE IV. Theoretical results obtained by fitting the data of Beurtey *et al.* (reference 15) on separated isotopes of Zn at 11.1 MeV.

A (amu)	V_S (MeV)	W_D (MeV)	β	σ_A (mb)	$\sigma_{in}{}^{2+}$ (mb)
64	49.9	9.0	0.27	850.6	52.2
66	50.8	10.5	0.23	885.1	34.8
68	50.9	12.2	0.20	913.2	22.7

The last experiment to be considered is on Ni^{60} at an incident proton energy of 30.8 MeV. The data were taken by Devins *et al.*[16] Here we have a test of the possibility of extrapolating Eqs. (45) and (46) to higher energies. The standard parameters of Table I were employed once more and V_S, W_D, and β were automatically varied by the search routine in order to obtain a fit to the data. The fit found for this case was not quite as good as the ones obtained for the lower energy differential cross sections. The results of the calculations and the experimental data are presented in Fig. 9. For the absorptive potential depth we obtained $W_D=11.9$ MeV. This indicates that the surface imaginary potential is in the range given by Eq. (46) and hence there is no marked tendency for W_D to change with energy. The derived value for the real potential depth was $V_S=44.9$ MeV which may be compared with the values predicted by Eq. (45) at $E=30.8$ MeV, i.e., $V_S=44\pm1$ MeV. Hence, we may say that Eqs. (45) and (46) can be used with some confidence to predict potential parameters at least up to an incident proton energy of 30 MeV and for nuclei in this mass region.

The fitting of the inelastic differential cross section yielded a deformation parameter of $\beta=0.14$. This is considerably lower than the Coulomb excitation value for Ni^{60}, which is $\beta\approx0.20$. However, the errors quoted for the inelastic measurements are rather large. Also we

[16] D. W. Devins, H. H. Forster, and G. G. Gigas, Nucl. Phys. **35**, 617 (1962).

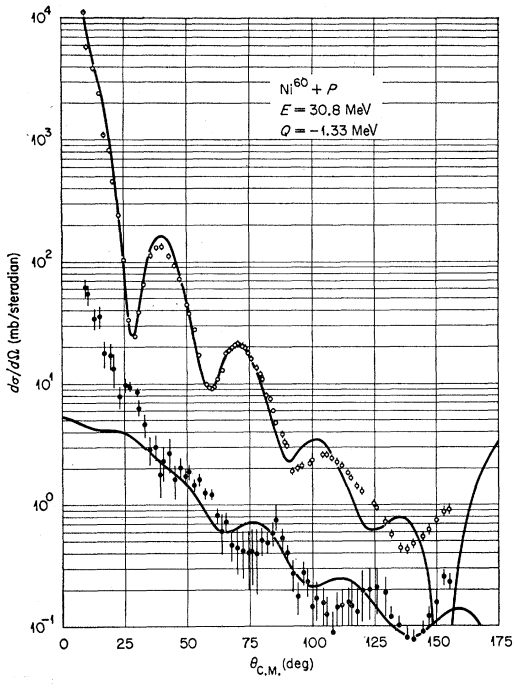

FIG. 9. Comparison of theory and experiment for Ni^{60} at 30.8 MeV. Table I gives the fixed model parameters. See text for discussion of results for the varied parameters.

see that the experimental and theoretical 2^+ reaction cross sections diverge appreciably at forward angles. The theoretical results for the elastic scattering do not reproduce the experimental data very well at large scattering angles. This may indicate the necessity of including some volume absorption in the model at higher energies.

4. SUMMARY AND CONCLUSIONS

We have shown in this paper that the strong coupling theory of direct interactions, with inclusion of spin-orbit coupling, is able to give a unified treatment of the elastic scattering of protons and the inelastic scattering leading to low-lying collective states. However, great care is necessary in the interpretation of the experimental data and the theoretical results when the incident proton energy is less than about 5 MeV above the nuclear (p,n) threshold energy. If a fixed set of geometrical optical parameters and a fixed spin-orbit strength are used, then the elastic scattering distributions can be reproduced excellently for a range of medium-mass nuclei, while the theoretical 2^+ differential cross sections are in good qualitative agreement with the available data.

The data analysis determines the assumed surface absorption potential depth only within about 15% of the value $W_D=10.6$ MeV and there are considerable individual fluctuations. The real Saxon potential depth at each energy has been found to be within 2% of the values represented by Eq. (45) and this formula can be extrapolated to higher energies. But at energies greater than 20 MeV, it may be necessary to introduce some volume absorption into the model. This remains to be investigated when more extensive higher energy experimental measurements become available.

It has proved possible to derive, from the inelastic scattering data, fairly good values for the nuclear distortion parameters β. For values of β greater than about $\beta=0.2$, it seems necessary to use the coupled equations approach rather than the DWBA formalism, although this latter theory is capable of giving good fits to the inelastic angular distribution shapes. When $\beta>0.2$, the presence of nuclear deformability begins to affect the elastic scattering and it is not possible to take account of this easily within the framework of the DWBA calculations. Also, for a given value of β, the DWBA treatment overestimates the magnitude of the inelastic cross section.

The values of β obtained in this work are, in general, consistent with those derived by electromagnetic methods, i.e., by Coulomb excitation and lifetime measurements. The β's obtained from $B(E2)$ determinations were found by assuming a quadrupole distorted, sharp edge charge distribution with an average radius given by $R_c=1.2A^{1/3}$. This is a rather crude model, but it is adequate for the rough comparisons discussed in the paper. On the whole, the agreement between the electromagnetic deformabilities and those found from inelastic scattering indicates that the collective model considerations of Sec. 2 represent a valid way to compute 2^+ reaction cross sections. In addition, the preliminary analysis of the data discussed in Sec. 3A showed that the parameters of the coupling form factors should be closely the same as the corresponding parameters of the real Saxon potential. This is predicted by the simple vibrational model calculations of Sec. 2A. Hence, we have evidence for the validity of the collective model.

In order to clear up various ambiguities in the calculations, it is necessary for the proton experiments to be extended to higher energies and performed for a much wider range of even-even nuclei, preferably separated isotopes. Data on 3^- angular distributions, as well as on the elastic and 2^+ differential cross sections, would be desirable.

In conclusion, we may say that the generalized optical model appears to be a useful way of correlating experimental data and studying the properties of nuclear collective states. Further applications of the model have been discussed elsewhere.[17,18]

ACKNOWLEDGMENTS

It is a pleasure to thank Dr. F. Perey and Dr. G. R. Satchler for many discussions and comments on this work. The computer program was written by D. E. Arnurius.

[17] B. Buck and F. Perey, Phys. Rev. Letters **8**, 444 (1962).
[18] B. Buck, Phys. Rev. **127**, 940 (1962).